JACS
JOURNAL OF THE AMERICAN CHEMICAL SOCIETY
Article
pubs.acs.org/JACS

Structure and Chemistry of the Heteronuclear Oxo-Cluster $[VPO_4]^{\bullet+}$: A Model System for the Gas-Phase Oxidation of Small Hydrocarbons

Nicolas Dietl,[†] Torsten Wende,[‡] Kai Chen,[§] Ling Jiang,[‡] Maria Schlangen,*[,†] Xinhao Zhang,[§] Knut R. Asmis,*[,‡] and Helmut Schwarz*[,†]

[†]Institut für Chemie, Technische Universität Berlin, Straße des 17. Juni 135, D-10623 Berlin, Germany

[‡]Fritz-Haber-Institut der Max-Planck-Gesellschaft, Faradayweg 4-6, D-14195 Berlin, Germany

[§]Lab of Computational Chemistry and Drug Design, Laboratory of Chemical Genomics, Shenzhen Graduate School of Peking University, Shenzhen 518055, P. R. China

Supporting Information

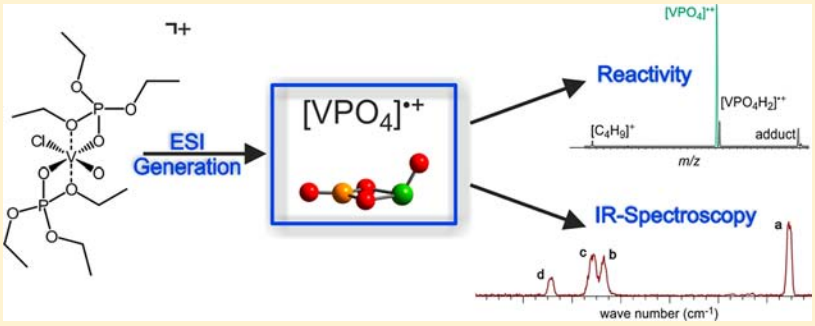

ABSTRACT: The heteronuclear oxo-cluster $[VPO_4]^{\bullet+}$ is generated via electrospray ionization and investigated with respect to both its electronic structure as well as its gas-phase reactivity toward small hydrocarbons, thus permitting a comparison to the well-known vanadium-oxide cation $[V_2O_4]^{\bullet+}$. As described in previous studies, the latter oxide exhibits no or just minor reactivity toward small hydrocarbons, such as CH_4, C_2H_6, C_3H_8, n-C_4H_{10}, and C_2H_4, while substitution of one vanadium by a phosphorus atom yields the reactive $[VPO_4]^{\bullet+}$ ion; the latter brings about oxidative dehydrogenation (ODH) of saturated hydrocarbons, e.g., propane and butane as well as oxygen-atom transfer (OAT) to unsaturated hydrocarbons, e.g. ethene, at thermal conditions. Further, the gas-phase structure of $[VPO_4]^{\bullet+}$ is determined by IR photodissociation spectroscopy and compared to that of $[V_2O_4]^{\bullet+}$. DFT calculations help to elucidate the reaction mechanism. The results underline the crucial role of phosphorus in terms of C−H bond activation of hydrocarbons by mixed VPO clusters.

1. INTRODUCTION

In terms of selective oxidation of hydrocarbons, oxygen-based systems represent a keystone in contemporary catalysis.[1−3] However, compared with the extensive application in industrial and academic research, a detailed mechanistic knowledge of the elementary processes and a complete understanding of the functional and structural properties of the reactive sites of e.g. solid-state catalysts are still rather limited.[4−6] In fact, contemporary heterogeneous catalysts are often composed of multiple components, i.e., mixed-metal oxo-frameworks, or noninnocent support materials are employed.[7−9] The efficient chemical transformation of n-butane to maleic anhydride by the so-called VPO catalysts (see Scheme 1) may serve as a well-known example for such a multicomponent system in heterogeneous catalysis. The catalysts are usually rather complex and composed of multiple VPO modifications, such as VPO_5 or $V_2P_2O_7$ phases; they facilitate the selective abstraction of eight hydrogen atoms from as well as the transfer of three oxygen atoms to n-C_4H_{10}. Quite likely, this large-scale transformation constitutes one of the most complex and yet highly selective

Scheme 1. Industrial Synthesis of Maleic Anhydride from n-Butane

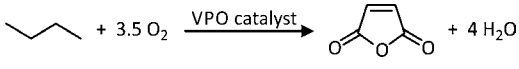

oxidation reactions used in industry today.[10−14] Since the first commercial use of VPO catalysts for the synthesis of maleic anhydride in the early 1980s, numerous experimental and theoretical studies have been carried out aimed at a better understanding of this remarkable process.[15−21] However, the underlying reaction mechanisms are still only poorly understood, and there is no shortage of speculations and hypotheses.[20]

Over the last decades the investigation of small cluster systems, in particular metal and metal oxide species, using advanced mass spectrometric methods in conjunction with theoretical studies, proved useful in unfolding insights at a

Received: January 10, 2013
Published: February 12, 2013

   dx.doi.org/10.1021/ja400198y | J. Am. Chem. Soc. 2013, 135, 3711−3721

molecular level; this includes reactivity studies of ion/molecule reactions[22−32] as well as recent advantages in the development of gas-phase infrared photodissociation spectroscopy.[33−39] Due to their large application in heterogeneous catalysis, especially vanadium oxides have been studied exhaustively, and a remarkable reactivity toward small hydrocarbons has been uncovered.[25,27,30,37,40−47] With respect to the VPO catalysts, it was conjectured, based on gas-phase as well as surface studies, that the structurally often ill-defined phosphate species work as catalytically innocent linkers between the active vanadium-oxide sites in mixed metal-oxide phosphates.[10] However, this assumption was questioned by several gas-phase studies on the open-shell oxide cation $[P_4O_{10}]^{\bullet+}$, in which the efficient thermal activation of even methane and other small, inert hydrocarbons at ambient conditions by the metal-free oxide was demonstrated with an even higher reactivity of $[P_4O_{10}]^{\bullet+}$ toward CH_4 compared to the isostructural, metallic analogue $[V_4O_{10}]^{\bullet+}$.[48−50] Further studies aimed at a more systematic investigation of mixed vanadium−phosphorus oxygen cluster ions $[V_xP_{4-x}O_{10}]^{\bullet+}$ (x = 1−3).[51,52] As shown by a theoretical analysis, these systems possess an oxygen-centered radical which has been found to be crucial in terms of hydrogen-atom transfer (HAT) from methane;[53] for all $[V_xP_{4-x}O_{10}]^{\bullet+}$ (x = 1−3) clusters, the structure possessing the lowest energy corresponds to the P−O$^{\bullet}$ isomer, i.e., the spin density is mostly localized at the phosphorus-bound, terminal oxygen atom. Despite their high reactivity, the $[V_xP_{4-x}O_{10}]^{\bullet+}$ (x = 2−3) clusters are nevertheless very selective in their reactions with ethane and ethene, and this chemoselectivity markedly depends on the composition of the tetranuclear cage cluster. Because the low-lying empty 3d-orbitals of vanadium can better stabilize the radical site formed in the course of reductive processes, the presence of vanadium in the cluster favors the formation of an open-shell product ion generated, e.g., in the oxidative dehydrogenation; in contrast, phosphorus rather promotes the formation of a closed-shell product cluster, e.g., in the course of HAT.[54]

In view of the fact that the "real world" VPO catalysts consist of multiple components, including fully oxidized VPO_5 as well as lower oxidized $V_2P_2O_7$ phases,[10] it deems of interest to extend the scope of the reactivity studies to only partially oxidized systems; in $[V_xP_{4-x}O_{10}]^{\bullet+}$ (x = 2−3) the P and V atoms are oxidized to the highest oxidation state of +V considering a terminal O$^{\bullet-}$ unit in the cluster. As an example for lower oxidized metal oxides, the small vanadium(IV/V)-oxide cation $[V_2O_4]^{\bullet+}$ has been studied extensively, including its structural characterization;[37] further, it has been shown that this oxide cation exhibits no reactivity in terms of ODH and OAT toward small hydrocarbons, such as CH_4, C_2H_6, C_3H_8, n-C_4H_{10}, and C_2H_4.[40] Regarding its electronic structure, $[V_2O_4]^{\bullet+}$ possesses no spin density at one of the oxygen atoms; instead, the unpaired electron in $[V_2O_4]^{\bullet+}$ is centered at one vanadium atom, thus corresponding to a mixed valence cluster $[V^{IV}V^{V}O_4]^{\bullet+}$.

Here, we report on the generation of the small, heteronuclear oxo cluster $[VPO_4]^{\bullet+}$ by electrospray ionization (ESI), its electronic structure in the gas phase as well as its reactivity toward small hydrocarbons. The results are compared to the reactivity and structure of the gaseous vanadium-oxide cation $[V_2O_4]^{\bullet+}$ aimed at uncovering the underlying doping effects in terms of C−H bond activation of small hydrocarbons. As shown recently, substitutions of an atom by another element significantly affects the gas-phase ion chemistry of various cluster systems.[55−59]

2. METHODS

2.1. Experimental Details. The reactivity studies and the collision-induced dissociation (CID) experiments were carried out using a tandem mass spectrometer with QHQ configuration (Q: quadrupole, H: hexapole) equipped with an electrospray ionization (ESI) source as described elsewhere.[60] Briefly, the $[VPO_4]^{\bullet+}$ cluster was generated by ESI of a millimolar solution of $VOCl_3$ and $PO(OEt)_3$ (both purchased from Sigma-Aldrich) in methanol, which were introduced through a fused-silica capillary to the ESI source by a syringe pump (~3 μL min^{-1}). Nitrogen was used as nebulizing and drying gas at a source temperature of 80 °C. Maximal yield of the desired oxide cation was achieved by adjusting the cone voltage (U_C) to 140 V; U_C determines the degree of collisional activation of the incident ions in the transfer from the ESI source to the mass spectrometer.[61] The $[V_2O_4]^{\bullet+}$ cluster was generated by ESI of a millimolar solution of $VO(O^iPr)_3$ and U_C = 150 V.[62,63] Next, the desired ion was mass selected using Q1 and reacted with the neutral gas in the hexapole at pressures on the order of 10^{-4} mbar; this corresponds approximately to single-collision conditions.[60,64] The ion/molecule reactions were probed at a collision energy (E_{lab}) set to nominally 0 eV, which in conjunction with the ~0.4 eV kinetic energy width of the parent ion at peak half-height[60] allows the investigation of quasithermal reactions, as demonstrated previously;[65−67] moreover, it was shown in many studies that also fragment ions generated after multiple fragmentation processes at harsher ionization conditions undergo quasithermal ion/molecule reactions.[66,68−71] Previous studies on the reactivity of $[VPO_4]^{\bullet+}$ are not known to our knowledge; thus, an exact temperature of the ions cannot be predicted. However, no reactivity of $[V_2O_4]^{\bullet+}$ toward small hydrocarbons is observed using our experimental setup as found in previous studies. The similar ionization procedure suggests that also the $[VPO_4]^{\bullet+}$ ions can be assumed as thermal. Further, the reactivity of $[VPO_4]^{\bullet+}$ toward small hydrocarbons is not affected using various cone voltages in the range of 120−170 V. Finally, the exothermicity of the processes described in the following is further confirmed by increasing the collision energy resulting in a depletion of the respective product channel. CID experiments were probed at different collision energies E_{lab} between 0 and 25 eV, and xenon was used as a collision gas. Finally, the reaction was followed by detection of the ionic products by scanning Q2.

The infrared photodissociation (IRPD) experiments were carried out using an ion trap−tandem mass spectrometer.[72,73] Gas-phase ions are produced in a commercial Z-spray ESI source. The beam of ions passes a 4 mm skimmer, is then collimated in a radio frequency (RF) decapole ion guide, and enters a quadrupole mass filter that serves to mass-select the $[VPO_4]^{\bullet+}$ parent ions. These are subsequently focused into a cryogenically cooled RF ring electrode ion trap. The trap is continuously filled with a helium buffer gas at an ion trap temperature of 15 K, allowing for the accumulation and thermalization of the ions. Inside the ion trap, the mass-selected $[VPO_4]^{\bullet+}$ ions undergo three-body collisions with the buffer gas which promote the formation of weakly bound ion−He atom complexes. Under the present experimental conditions a distribution of helium-tagged complexes $[VPO_4]^{\bullet+}$−He_n is formed, ranging from n = 1−3 (Figure S1), with n = 2 corresponding to the most abundant species; these complexes are used for the IRPD measurements. After loading the ion trap for 98 ms, all ions are extracted and focused both temporally and spatially into the center of the extraction region of an orthogonally mounted linear time-of-flight (TOF) mass spectrometer. Here, the ion packet is irradiated with an infrared (IR) laser pulse, and high-voltage extraction pulses are applied for recording TOF mass spectra. Pulsed IR radiation is provided by a tabletop OPO/OPA/$AgGaSe_2$ IR laser system (LaserVision)[74] which is pumped by a pulsed, seeded Nd:YAG laser (Continuum, Powerlite P-8000). The pump laser operates at a repetition rate of 10 Hz and provides 7 ns long pulses. The IR laser system is operated in the spectral region from 800 to 1500 cm^{-1}, in which IR pulses with pulse energies ≤4 mJ and a spectral bandwidth of ~1.8 cm^{-1} are typically produced.

Measuring an IRPD spectrum of each complex $[VPO_4]^{\bullet+}$−He_n with n = 1−3 individually is generally not straightforward. All of these complexes are present in the ion packet, which is extracted from the

dx.doi.org/10.1021/ja400198y | J. Am. Chem. Soc. 2013, 135, 3711−3721

trap and simultaneously interact with the IR laser pulse. When the laser is on resonance with a vibrational transition, all ions can dissociate, e.g., via loss of He atoms, which may lead to a "cross-talk" between the different dissociation channels. For example, the n = 2 mass channel may contain contributions from both parent and photofragment ions, i.e., the n = 2 complex can dissociate into lighter species (n = 0, 1) and the former can be formed by dissociation of the heavier complex n = 3. This makes the distinction of ion signals into parent and fragment ions ambiguous. In the present experiment, this problem is solved by irradiating the ion packet during the acceleration phase in the TOF mass spectrometer, i.e., the IR laser pulse is applied ~1 μs after the high-voltage extraction pulses. As a consequence, parent and photofragment ions of identical mass acquire different amounts of kinetic energy and thus lead to separate peaks in the TOF mass spectrum (see Figure S1), i.e., IRPD spectra can be measured background-free. This technique has been described earlier in IRPD studies on krypton-tagged suberate dianions.[73] IRPD spectra of the most abundant helium-tagged complexes n = 2 and 1 are measured. At typical pulse energies ≤4 mJ, IRPD of these complexes proceeds only via loss of one of more helium atoms (see Figure S1). TOF spectra are recorded 50−70 times for each wavelength step. IRPD spectra are obtained by plotting the relative photodissociation cross section σ according to $\sigma \propto -\ln[1 - I_F(\nu)/(I_F(\nu) + I_P(\nu))]/P(\nu)$ with the parent ion ($I_P(\nu)$) and photofragment ion ($I_F(\nu)$) intensities and the frequency-dependent laser pulse energy $P(\nu)$.

2.2. Computational Details. All calculations relevant for uncovering mechanistic details were performed using the Gaussian09 package.[75] Geometries were optimized at the unrestricted UB3LYP level of theory[76,77] with the triple-ζ plus polarization basis sets def2-TZVP.[78] Vibrational frequency analyses have been carried out at the same level of theory to characterize the nature of stationary points as minima or transition structures and to derive the zero-point energy (ZPE) corrections. All relative energies presented in this work are corrected for ZPE and given in kJ mol^{-1}. Intrinsic reaction coordinate (IRC)[79−81] calculations or manual displacements along the reaction trajectory of the imaginary frequency were performed to link all transition states with the respective intermediates. All given ionic reactants, intermediates, and transition states have been located on the ground-state doublet potential energy surface; selected structures optimized in the quartet state are 200 kJ mol^{-1} and more higher in energy; however, for **23** and **24** (Figure 4b), the splitting is with 7 and 26 kJ mol^{-1} relatively small. This further results in significant spin contamination for **23** ($\langle S^2\rangle$ = 1.72) and **24** ($\langle S^2\rangle$ = 1.73), while for all other structures spin contamination with a typical value of $\langle S^2\rangle$ = 0.76 is not a problem. For the IR-relevant structural assignment, the TURBOMOLE 6.2 program[82] is used. Here, the B3LYP+D(ispersion) model[76,77,83] is employed together with a triple-ζ valence basis set TZVPP.[84] Harmonic vibrational frequencies are obtained from analytic second derivatives.[85] Zero-point vibrational energy contributions have been taken into account for the determination of relative energies. It is known that B3LYP vibrational frequencies are systematically too large;[86,87] however, the agreement with observed frequencies can be improved by appropriate scaling. Scaling then accounts for both anharmonicities and systematic errors of the calculated harmonic force constants (calculated harmonic wavenumbers are compared to observed fundamentals including anharmonicities). We use scaling parameters that were determined for small vanadium oxide cluster cations.[88] The vanadyl (V = O) modes are scaled by 0.9167 and all other modes by 0.9832. The simulated linear absorption spectra are derived from scaled harmonic frequencies and intensities. The resulting stick spectra are convoluted using a Gaussian line shape function with a width of 10 cm^{-1} (fwhm) for better comparability.

3. RESULTS AND DISCUSSION

3.1. Generation of $[VPO_4]^{\bullet+}$. A large number of different ions are generated by ESI from a given solution, and the intensity of the ion of interest can be optimized by adjusting the ionization conditions. As mentioned in the Methods section, the most decisive parameter in this respect is the cone voltage U_C, which determines the extent of collisional fragmentation of the ions formed initially in the differentially pumped system of an ESI source. At low U_C values, solvated ions are formed, which then lose the weakly bound solvent molecules at increased cone voltages. This is followed by the evaporation of more strongly bound ligands including the cleavage of covalent bonds; finally, at rather high cone voltages even bare metal cations can be generated.[60] Further, by choosing the right precursor, also larger metal-oxide clusters are accessible, as shown previously for various vanadium systems;[62,89] these clusters are otherwise only accessible in the gas phase by use of laser vaporization/ionization sources. However, the generation of mixed, cationic oxo-clusters by ESI is rather unique.

Upon spraying a millimolar solution of commercially available vanadyl trichloride $VOCl_3$ and triethyl phosphate $PO(OEt)_3$ in methanol or acetonitrile, the cluster cation $[VPO_4]^{\bullet+}$ (m/z = 146 amu) is generated in excellent yields (Figure 1); the maximum intensity is achieved at U_C = 160 V. Regarding the genesis of $[VPO_4]^{\bullet+}$, a stepwise fragmentation from an *in situ* formed complex in solution is likely to occur. Based on CID experiments of the individual species involved, a fragmentation pathway for the generation of $[VPO_4]^{\bullet+}$ can be derived (Scheme 2). The ion $[VP_2O_3(OC_2H_5)_6Cl]^{\bullet+}$ (**1**) at m/z = 466 amu serves as the parent ion; most likely, it contains a Cl−V−O moiety with two triethyl-phosphate groups coordinated to the metal core (Scheme 2).[90] Hence, increasing the cone voltage to values >40 V initiates the breakdown of **1** (Figure 1), resulting first in the loss of neutral C_2H_5Cl and the formation of the vanadium complex $[VP_2O_4(OC_2H_5)_5]^{\bullet+}$ (**2**); further fragmentations involve the consecutive elimination of C_2H_4 (Δm = 28) via **2** → $[VP_2O_4(OH)(OC_2H_5)_4]^{\bullet+}$ (**3**) → $[VP_2O_4(OH)_2(OC_2H_5)_3]^{\bullet+}$ (**4**) → $[VP_2O_4(OH)_3(OC_2H_5)_2]^{\bullet+}$ (**5**) → $[VP_2O_4(OH)_4(OC_2H_5)]^{\bullet+}$ (**6**). From the latter, the fragmentation pattern bifurcates into two different pathways (Scheme 2): The first one continues with the loss of C_2H_4 from the remaining ethoxy side chain, thus forming the oxo-/hydroxyl-complex ion $[VP_2O_4(OH)_5]^{\bullet+}$ (**7**) from which $[VP_2O_5(OH)_3]^{\bullet+}$ (**8**) and $[VP_2O_6(OH)]^{\bullet+}$ (**9**) are generated upon the stepwise expulsions of H_2O, respectively. In the final step, one of the remaining phosphate fragments in **9** is liberated as neutral HPO_3 (metaphosphoric acid) to form the ion of interest $[VPO_4]^{\bullet+}$ (**13**, m/z = 146 amu). The second pathway commences with the elimination of phosphorous acid H_3PO_4 from **6**, which then leads to the formation of $[VPO_3(OH)(OC_2H_5)]^{\bullet+}$ (**10**). Upon further collisional activation, expulsion of C_2H_4 to form $[VPO_3(OH)_2]^{\bullet+}$ (**12**) occurs, and finally loss of H_2O produces the target ion **13**. Moreover, structures **7** and **8** have been identified as direct precursors for **12** via losses of neutral H_3PO_4 and HPO_3, respectively. In addition, collision-induced elimination of HPO_3 from **7** gives rise to the formation of $[VPO_2(OH)_4]^{\bullet+}$ (**11**) which can consecutively undergo further dehydration to also produce **12**.

At cone voltages exceeding 160 V, the signal intensity of $[VPO_4]^{\bullet+}$ decreases again due to the dissociation of **13** into $[VO_2]^+$ (**14**) and $[VO]^+$ (**15**) (Figure 1), concomitant with the expulsion of open-shell oxides $PO_2^{\bullet}$ and $PO_3^{\bullet}$, respectively.

3.2. IRPD Spectrum and Structural Assignment. Figure 2 (top panel) shows the experimental IRPD spectrum of the $[VPO_4]^{\bullet+}$−He complex. It exhibits four absorption bands (labeled **a**−**d**) in the spectral region from 800 to 1500 cm^{-1}: The most intense band is observed at 1445 cm^{-1} (**a**) and three bands appear below 1100 cm^{-1}, i.e., at 1064 (**b**), 1038 (**c**) and 953 cm^{-1} (**d**). Addition of a second He atom only affects the

dx.doi.org/10.1021/ja400198y | J. Am. Chem. Soc. 2013, 135, 3711−3721

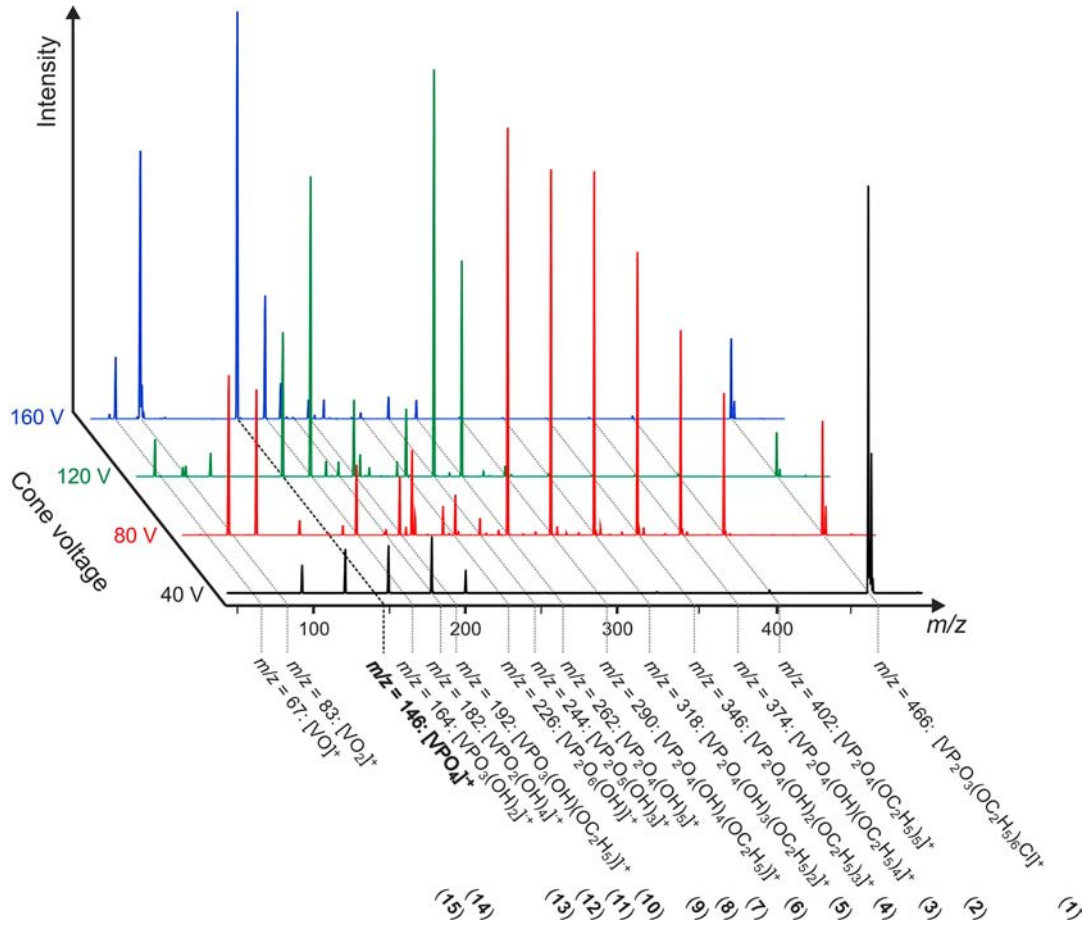

Figure 1. Mass spectra of a solution of $VOCl_3$ and $PO(OEt)_3$ in CH_3OH at various cone voltages. Structural assignments are based on the breakdown processes depicted in Scheme 2.

Scheme 2. Postulated Fragmentation Mechanism for the Generation of $[VPO_4]^{\bullet+}$ (13) from Precursors $VOCl_3$ and $PO(OEt)_3$[a]

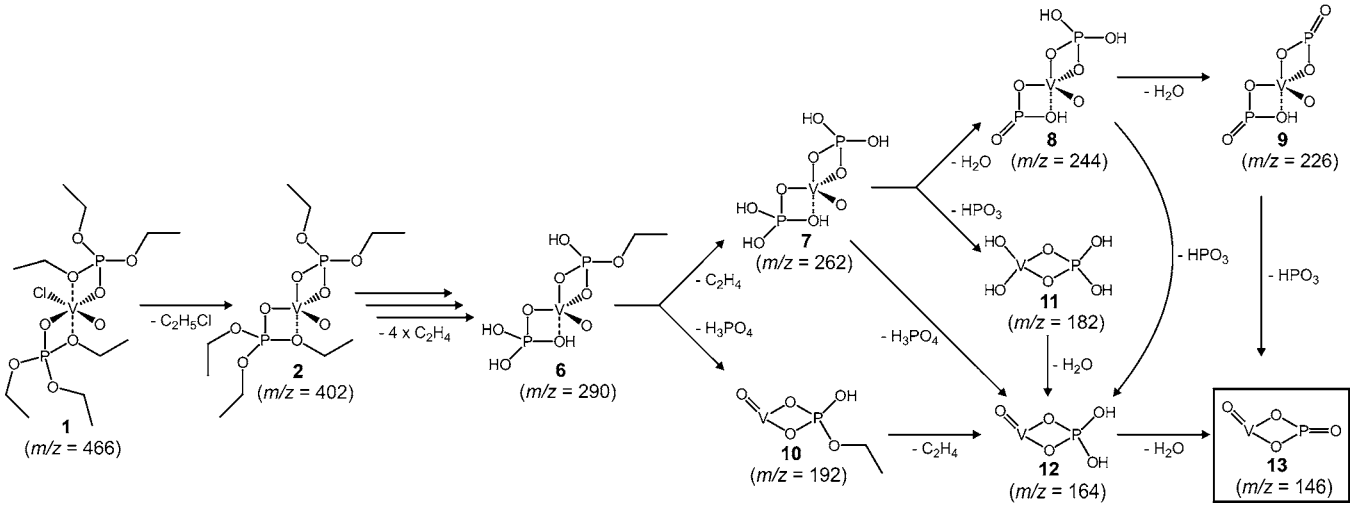

[a]The observed cone voltage induced in-source dissociation has been verified with further CID experiments of the respective ions. For the sake of clarity, the positive charge is omitted for all species.

position of bands c and d, which are shifted to higher energies by 5 and 4 cm^{-1}, respectively.

A preliminary assignment of bands **a**–**d** can be made based on a comparison to the IRPD spectra of $[V_2O_4]^{\bullet+}$–He_3[88] and $[CeVO_4]^{\bullet+}$–He,[91] which both were found to have M–$(O)_2$–M ring structures containing two terminal M═O bonds in *trans* configuration. Both IRPD spectra exhibit bands only below 1050 cm^{-1}; the characteristic vanadyl (V═O) stretching modes are observed above ($[V_2O_4]^{\bullet+}$–He_3: 1029, 1049 cm^{-1}; $[CeVO_4]^{\bullet+}$–He: 1017 cm^{-1}) and the M–$(O)_2$–M ring modes below 1000 cm^{-1}. As phosphorus has a considerably smaller mass compared to vanadium, all corresponding modes

dx.doi.org/10.1021/ja400198y | J. Am. Chem. Soc. 2013, 135, 3711–3721

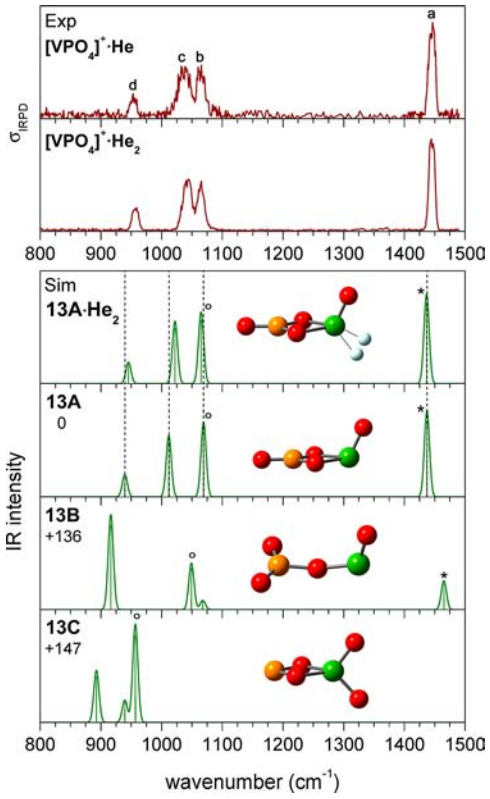

Figure 2. Experimental IRPD spectra (top) of the ion–He complexes $[VPO_4]^{\bullet+}$–$He_{1,2}$ compared to simulated B3LYP+D/TZVPP linear absorption spectra of three bare isomers (**13A**–**C**) and the helium-tagged isomer **13A·He$_2$**. Given values indicate the relative energies (in kJ mol^{-1}) of the optimized structures **13A**–**C** (yellow, P; green, V; red, O; gray, He). The V═O stretching modes are marked with a circle, and P═O modes with an asterisk. Harmonic frequencies of the V═O modes are scaled by 0.9167 and all other modes by 0.9832.

are expected to be significantly shifted to higher wavenumbers. For example, the P═O stretching vibrations of the phosphonate group ($-PO_3H_2$) are typically located in the spectral range from 1150 to 1270 cm^{-1}.[92,93] Therefore our preliminary assignment is as follows: the P═O stretching mode is expected at the highest wavenumber followed by the V═O stretching and P–$(O)_2$–V ring modes, and we tentatively assign bands **a**–**d** accordingly. Furthermore, the observation that upon addition of a second He atom only bands **c** and **d** are affected suggest that the He atom binds to one of the ring atoms, most probably the V atom, and therefore, as a result of a cage-like effect, blue shifts mainly those bands (bands **c** and **d**).

To allow for an unambiguous structural assignment, the experimental IRPD spectra of $[VPO_4]^{\bullet+}$–$He_{1,2}$ are compared to simulated B3LYP+D/TZVPP linear absorption spectra of three stable structures (**13A**–**C**, Figure 2). The lowest energy structure found for $[VPO_4]^{\bullet+}$ is characterized by a four-membered V–$(O)_2$–P ring containing terminal V═O and P═O bonds (**13A**, Figure 2); this bonding pattern is similar to the previously reported structures for $[Zr_2O_4]^{\bullet+}$,[33] $[V_2O_4]^{\bullet+}$,[88] or $[CeVO_4]^{\bullet+}$.[91] The other isomers considered are predicted to lie >100 kJ mol^{-1} higher in energy, ruling these out as possible candidates purely for energetic reasons. This includes the isomer with a chain-like structure (**13B**, +136 kJ mol^{-1}) or the cyclic structure containing a terminal VO_2 group (**13C**, +147 kJ mol^{-1}). The experimental spectrum is in excellent agreement with the simulated spectrum of the lowest energy structure **13A**, both for the band positions (exp/sim: 1445/1437 cm^{-1} (**a**), 1064/1069 cm^{-1} (**b**), 1043/1012 cm^{-1} (**c**), 957/939 cm^{-1} (**d**)) as well as their relative intensities, respectively. On the other hand, nonsatisfactory agreement with the experimental spectrum is found for isomers **13B** and **13C.** The observed bands **a**–**d** are thus assigned as follows: **a** and **b** are attributed to terminal P═O and V═O stretching vibrations, respectively, while the bands **c** and **d** correspond to the in-plane deformation modes of a V–$(O)_2$–P ring. Moreover, an even better agreement between the experimental and simulated vibrational frequencies is obtained, when the ion–He atom interactions are taken into account in the calculations. Both He atoms are predicted to bind to the V atom (in isomer **13A**), each with a binding energy of 14 kJ mol^{-1} (structure **13A·He$_2$**, Figure 2). Normal-mode analysis confirms that the presence of the helium atoms particularly affects the vibrational frequencies of the ring vibrations. In contrast, the position of the P═O and V═O stretching bands (**a** and **b**) are predicted to remain unchanged upon tagging, confirming the experimental observation.

3.3. Reactivity of $[VPO_4]^{\bullet+}$ with Small Hydrocarbons.

As mentioned previously, the homonuclear cationic cluster $[V_2O_4]^{\bullet+}$ was found to be rather inert toward small hydrocarbons, e.g., CH_4, C_2H_6, C_3H_8, *n*-C_4H_{10}, and C_2H_4.[40] We confirmed these results in experiments performed exemplarily for the $[V_2O_4]^{\bullet+}$/*n*-C_4H_{10} couple in our experimental setup; here, no bond activation of *n*-butane serving as least inert substrate investigated occurs, and only adduct formation can be observed. However, the reactivity patterns change significantly when one of the vanadium atoms is replaced by phosphorus (eqs 1–5, Figure 3).

$$[VPO_4]^{\bullet+} + CH_4 \longrightarrow \textit{no reaction} \quad (1)$$

$$[VPO_4]^{\bullet+} + C_2H_6 \longrightarrow [VPO_4C_2H_4]^{\bullet+} + H_2 \quad (2)$$

$$[VPO_4]^{\bullet+} + C_3H_8 \longrightarrow [VPO_4H_2]^{\bullet+} + C_3H_6 \quad (3a)$$

$$\longrightarrow VPO_4H^{\bullet} + [C_3H_7]^{+} \quad (3b)$$

$$[VPO_4]^{\bullet+} + n\text{-}C_4H_{10} \longrightarrow [VPO_4H_2]^{\bullet+} + C_4H_8 \quad (4a)$$

$$\longrightarrow VPO_4H^{\bullet} + [C_4H_9]^{+} \quad (4b)$$

$$[VPO_4]^{\bullet+} + C_2H_4 \longrightarrow [VPO_3]^{\bullet+} + C_2H_4O \quad (5)$$

As found for $[V_2O_4]^{\bullet+}$, also $[VPO_4]^{\bullet+}$ does not react with methane, and only very inefficient H_2 elimination is observed beside adduct formation in the thermal reaction with ethane (Figure 3a and Table 1). For the higher homologues propane or *n*-butane, however, oxidative dehydrogenation takes place with increasing reaction rates (Table 1), resulting in the formation of the reduced cluster ion $[VPO_4H_2]^{\bullet+}$ and neutral C_3H_6 or C_4H_8, respectively, eqs 3a and 4a. In addition, hydride abstraction is observed for both couples $[VPO_4]^{\bullet+}$/C_3H_8 and $[VPO_4]^{\bullet+}$/C_4H_{10}, leading to the formation of the neutral radical $VPO_4H^{\bullet}$ and the carbenium ions $[C_3H_7]^{+}$ and $[C_4H_9]^{+}$, respectively, eqs 3b and 4b. Further, the reaction with unsaturated hydrocarbons, e.g., ethene, gives rise to oxygen-atom transfer to the hydrocarbon with $[VPO_3]^{\bullet+}$ being formed as ionic product, eq 5. Regarding the relative rate constants for bond activation, the reaction proceeds most efficiently with *n*-butane and decreases when going from propane via ethene to ethane (Table 1).

dx.doi.org/10.1021/ja400198y | J. Am. Chem. Soc. 2013, 135, 3711–3721

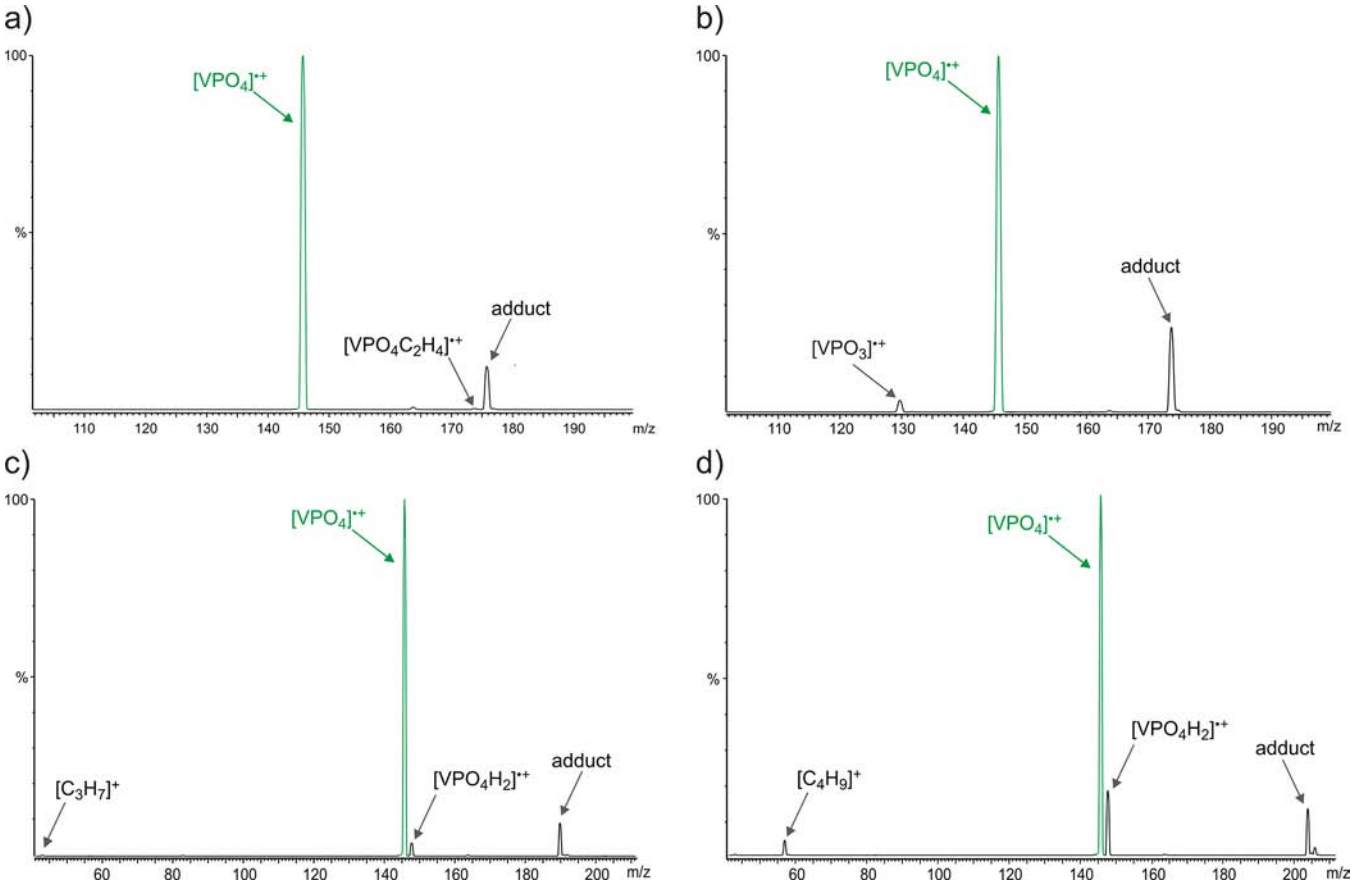

Figure 3. Ion/molecule reactions of mass-selected $[VPO_4]^{\bullet+}$ with (a) C_2H_6, (b) C_2H_4, (c) C_3H_8, and (d) n-C_4H_{10} (in the range of $3-5 \times 10^{-4}$ mbar). The weak signal at m/z = 164 amu observed in all four spectra is due to adduct formation of the parent ion with residual water molecules present as impurity within the vacuum region.

Table 1. Relative Rate Constants for the Overall Reactions, k_{rel}, and Neglecting Adduct formation, k_{rel}*, As Well As the Product Distribution for the Ion/Molecule Reactions of $[VPO_4]^{\bullet+}$ with Small Hydrocarbons[a]

			product channel				
neutral reactant	k_{rel}	k_{rel}*	ODH	OAT	H^- transfer	dehydrogenation	adduct formation
C_2H_4	98	23	–	21	–	–	79
C_2H_6	46	2	–	–	–	3	97
C_3H_8	79	26	39	–	3	–	58
n-C_4H_{10}	100	100	56	–	9	–	35

[a]Relative rate constant values are normalized to k_{rel} = 100 for the reaction of $[VPO_4]^{\bullet+}$ with n-C_4H_{10}. Product distribution values are normalized to $\sum$ = 100; branching ratio is obtained via linear regression ($p_{reactant}$ = 0). ODH: oxidative dehydrogenation; and OAT: oxygen-atom transfer.

Mechanistic insights into the oxidative dehydrogenation can be obtained from deuterium-labeling experiments. For the oxidation of propane, the reaction of $[VPO_4]^{\bullet+}$ with $CH_3CD_2CH_3$ gives rise exclusively to the ionic cluster $[VPO_4HD]^{\bullet+}$; $[VPO_4H_2]^{\bullet+}$ and $[VPO_4D_2]^{\bullet+}$ are not observed. Hence, the elimination proceeds in a clean 1,2-fashion without any H/D scrambling processes involved. This holds presumably also true for the reaction with deuterium-labeled butane, i.e., $CD_3(CH_2)_2CD_3$; here, $[VPO_4HD]^{\bullet+}$ and $[VPO_4H_2]^{\bullet+}$ are the only product ions generated with a relative branching ratio of 1:1.4. With respect to the hydride-transfer channel, i.e., the formation of the carbenium ions $[C_3H_7]^+$ and $[C_4H_9]^+$, the abstraction from the secondary position is clearly favored. The product distributions of VPO_4H versus VPO_4D amount to 11:1 and >20:1 (1:>20) for the reaction of $[VPO_4]^{\bullet+}$ with $CD_3(CH_2)_2CD_3$ and $CD_3CH_2CD_3$ ($CH_3CD_2CH_3$), respectively; for the deuterated propanes, the small branching ratio for the hydride abstraction does not permit to accurately determine the site selectivity.

3.4. Mechanistic Aspects. To obtain further information on the reaction mechanisms, quantum-chemical calculations have been carried out for the reactions of $[VPO_4]^{\bullet+}$ with ethene and propane, respectively.

Chemically reasonable structures for C_2H_4O, generated according to eq 5, are oxirane, vinyl alcohol, and acetaldehyde. Among them, acetaldehyde corresponds to the thermochemically most favored neutral product and has been shown to be generated in many OAT reactions of oxo-clusters with ethene.[43,69,94−96] This holds true for the reaction of $[VPO_4]^{\bullet+}$ toward ethene as well; while the generation of acetaldehyde is exothermic (−38 kJ mol^{-1}), both epoxidation of C_2H_4 to give ethylene oxide as well as the formation of vinyl alcohol are endothermic (+85 and +14 kJ mol^{-1}, respectively).

dx.doi.org/10.1021/ja400198y | J. Am. Chem. Soc. 2013, 135, 3711−3721

Furthermore, the reaction takes place solely at the P═O moiety; transfer of an oxygen atom from the V═O site to generate acetaldehyde is +175 kJ mol^{-1} above the entrance channel and thus not accessible under thermal conditions.

The computed potential energy surface (PES) for the reaction of $[VPO_4]^{\bullet+}$ with C_2H_4 is given in Figure 4a. In the first step,

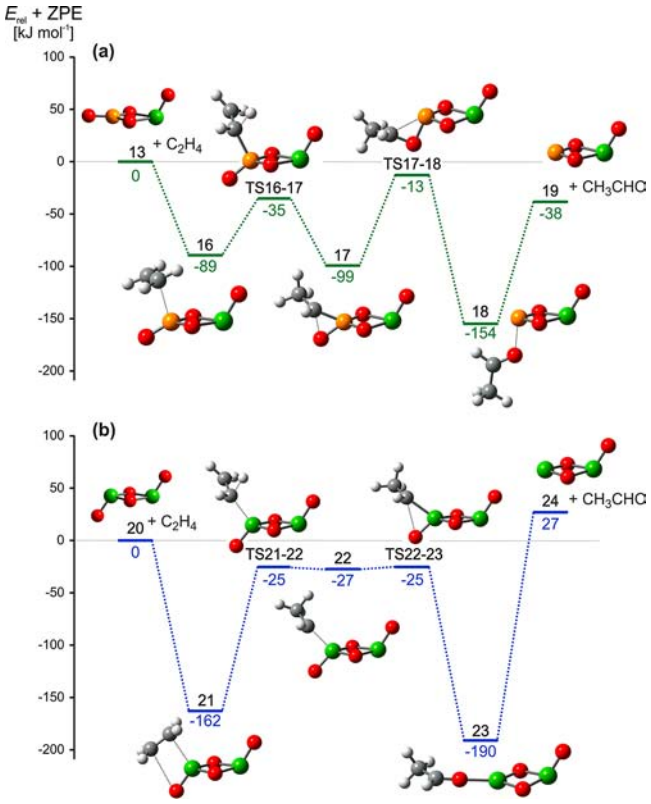

Figure 4. Simplified, electronic ground-state PESs for the reactions of (a) $[VPO_4]^{\bullet+}$ and (b) $[V_2O_4]^{\bullet+}$ with C_2H_4, calculated at the B3LYP/def2-TZVP level of theory (green, V; yellow, P; red, O; gray, C; white, H). The relative energies are given in kJ mol^{-1} and corrected for unscaled ZPE contributions.

a carbon atom of ethene coordinates to the phosphorus atom of the cluster ion to form intermediate **16**; as a consequence, the C═C double bond of the incoming ligand becomes elongated from 1.32 Å in free ethene to 1.36 Å, and the coordinating carbon atom of C_2H_4 is slightly pyramidalized with dihedral angles D_{HCCH} of 9° and 11°. Also the phosphorus atom loses its planar coordination sphere initially present in structure **13**; the terminal P═O bond in **16** is bent by 31° out of the P(μ-O)$_2$V ring plane. The reaction proceeds with a [1,2]-hydrogen migration from the proximal to the terminal carbon atom via transition structure **TS16−17**. Concomitantly, the C and O atoms approach each other, and the resulting intermediate **17** contains a hypervalent, four-coordinated phosphorus atom, forming a phospha-oxa cyclopropane analogue. The C−O distance of 1.66 Å in **17** is longer than expected for a C−O single bond (e.g., 1.431 Å in free ethanol or 1.425 Å in free ethylene oxide);[97] a further approach of both atoms is only achieved in **TS17−18** and is accompanied with a substantial elongation of the P−C bond. The resulting transfer of the hydrocarbon fragment to the terminal oxygen atom is associated with an intrinsic activation barrier of 86 kJ mol^{-1}, located only −13 kJ mol^{-1} below the entrance channel. In **18**, the newly formed acetaldehyde molecule coordinates almost rectangularly to the plane of the four-membered ring P(μ-O)$_2$V ($\angle$VPO = 98°, r(P−O) = 2.03 Å). Finally, liberation of acetaldehyde requires 116 kJ mol^{-1} and completes the reaction with an overall exothermicity of −38 kJ mol^{-1}. The spin density of the various open-shell intermediates remains on the vanadium atom throughout the whole reaction.

To explain the different reactivity of $[V_2O_4]^{\bullet+}$ versus $[VPO_4]^{\bullet+}$, the PES of $[V_2O_4]^{\bullet+}$ with C_2H_4 has been computed and studied as well (Figure 4b). Here, the ethylene molecule coordinates via its carbon atoms simultaneously to both the terminal oxygen and the vanadium(V) atom carrying no spin density; formation of the encounter complex **21** is much more exothermic (−162 kJ mol^{-1}) compared to the generation of the phosphorus-containing analogue **16** (−89 kJ mol^{-1}). An adduct complex, structurally similar to **21**, has also been located for the $[VPO_4]^{\bullet+}/C_2H_4$ couple at a relative energy of −143 kJ mol^{-1} with the ethene molecule coordinating to the vanadium and not to the phosphorus site; however, the subsequent activation barrier for the [1,2]-hydrogen migration is 5 kJ mol^{-1} higher and also entropically disfavored compared to the entrance channel $[VPO_4]^{\bullet+}/C_2H_4$; thus, this pathway is not accessible under ambient conditions. The analogous intrinsic barrier for the pure vanadium system is also relatively high and amounts to 137 kJ mol^{-1}; however, the associated transition structure **TS21−22** is in this case 25 kJ mol^{-1} lower in energy compared to the entrance channel and is accessible. The so-formed intermediate **22** is only 2 kJ mol^{-1} lower in energy compared to the two associated transition structures **TS21−22** and **TS22−23**; in the latter, acetaldehyde is generated by reductive elimination thus forming complex **23**. In contrast to the phosphorus-containing system **18**, the acetaldehyde ligand in **23** coordinates in an in-plane fashion to the vanadium atom, and the bond-dissociation energy (BDE) of acetaldehyde to the $[V_2O_3]^{\bullet+}$ cluster is much higher compared to the respective BDE of the P containing species [BDE($[V_2O_3]^{\bullet+}$−acetaldehyde) = 217 kJ mol^{-1}, BDE($[VPO_3]^{\bullet+}$−acetaldehyde) = 116 kJ mol^{-1}]. Although the relative energies of structures **23** and **24** have to be considered with care due to a broken spin character (see Computational Details section), the qualitative picture of an endothermic OAT reaction from $[V_2O_4]^{\bullet+}$ to ethene does not change. In contrast, the overall reaction is by 38 kJ mol^{-1} exothermic for the mixed $[VPO_4]^{\bullet+}$ cluster, i.e., the reason for the deviating reactivities of $[V_2O_4]^{\bullet+}$ and $[VPO_4]^{\bullet+}$ with ethene is due to thermochemical reasons. These findings contrast with the results of previous studies on the reactions of the larger cluster ions $[V_xP_{4-x}O_{10}]^{\bullet+}$ (x = 0, 2−4) with ethene.[54] For these systems, OAT from a V−O group is energetically less demanding compared to the transfer of an oxygen atom from P−O. A closer look at the product ion explains these differences: the cleavage of the P−$O_t^{\bullet}$ bond in the larger clusters gives rise to a phosphorus-centered radical and results in the reduction of the P atom to a formal oxidation state of 4; for $[VPO_4]^{\bullet+}$ described in this study, the spin remains located at the V atom, and OAT from P−O corresponds to the more favored reduction $P^{+V} \rightarrow P^{+III}$.

In the initial step of the reaction of $[VPO_4]^{\bullet+}$ with C_3H_8, an intermediate is generated which indicates an incipient hydride transfer from the alkane to the P atom of the cluster (**25**, Figure 5a); the overall Mulliken atomic charge of the C3 unit in **25** amounts to 0.46, while the spin density is located at the remote V atom. The C−H bond is remarkably elongated from 1.09 Å in free propane to 1.24 Å in intermediate **25**, and the P−H bond amounts to 1.63 Å; the originally planar PO_3

dx.doi.org/10.1021/ja400198y | J. Am. Chem. Soc. 2013, 135, 3711−3721

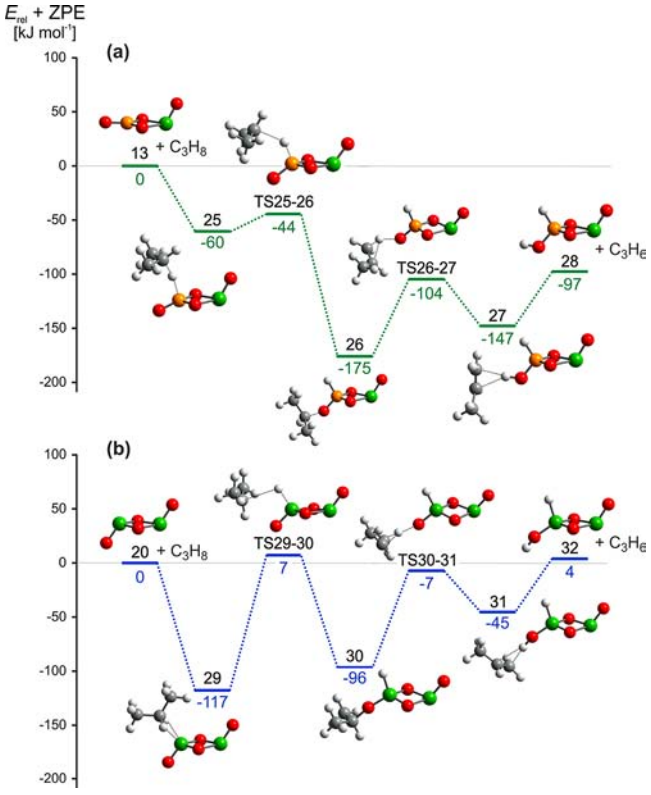

Figure 5. Simplified, electronic ground-state PESs for the reactions of (a) $[VPO_4]^{\bullet+}$ and (b) $[V_2O_4]^{\bullet+}$ with C_3H_8, calculated at the B3LYP/def2-TZVP level of theory (green, V; yellow, P; red, O; gray, C; white, H). The relative energies are given in kJ mol^{-1} and corrected for unscaled ZPE contributions.

unit of the cluster is bent by about 26° and the dihedral angle D_{CCCH} is slightly bent to 137°. The carbocationic character becomes even more pronounced in the subsequent transition structure **TS25−26** in which the Mulliken atomic charge at the C3 unit amounts to 0.80 and D_{CCCH} to 167°. Concomitant with the hydride transfer, the carbocation unit migrates via **TS25−26** to the terminal oxygen atom of the P−O unit, thus forming intermediate **26**; the P−H bond in the latter corresponds to a typical bond length for a P−H single bond ($r(P-H)_{[PH4]+}$ = 1.42 Å).[98] From intermediate **26**, a proton from one of the methyl groups is transferred to the oxygen atom via **TS26−27**, thus forming the hydrogenated product ion $[VPO_4H_2]^{\bullet+}$ to which neutral propene is loosely coordinated via the hydrogen atom of the newly formed hydroxy group. Finally, the reaction is completed by liberation of the propene fragment and generating the product ion **28**; the computed exothermicity of the overall reaction amounts to −97 kJ mol^{-1}.

As an alternative to the oxidative dehydrogenation, simple hydride transfer can occur as a competing pathway. The loss of the isopropyl cation $[C_3H_7]^+$ from intermediate **25** leads to the formation of the neutral, open-shell cluster $VPO_4H^{\bullet}$, and formation of $[i\text{-}C_3H_7]^+$ ion is associated with an overall exothermicity of −15 kJ mol^{-1}; a protonated cyclopropane isomer is 52 kJ mol^{-1} higher in energy and the primary $[n\text{-}C_3H_7]^+$ ion does not exist in the gas phase[99] but rearranges to either one of the two isomers.[100−103] The remarkably high selectivity toward the secondary C−H bond is in agreement with the hydride affinities of primary carbocations (derived by experimental $\Delta_f H$ data) which are ∼75−84 kJ mol^{-1} higher than for secondary carbocations.[104]

Again, a comparison of the reaction of $[V_2O_4]^{\bullet+}$ with C_3H_8 deems of interest to analyze the structure−reactivity relationship in more detail; the corresponding mechanism is given in Figure 5b. Here, the mode of coordination is distinctly different compared to the $[VPO_4]^{\bullet+}/C_3H_8$ couple; instead of forming one hydrogen bond, as described above for **25**, the C_3H_8 molecule coordinates to $[V_2O_4]^{\bullet+}$ via both C_{sec}−H bonds, thus forming a five-coordinated vanadium center (**29**, Figure 5b). Both C−H bonds are only slightly elongated to 1.12 Å, while the H−C−H angle is bent to ∠HCH = 113°. As found for **TS25−26** of the mixed vanadium−phosphorus system, a hydride transfer together with the migration of a carbocationic C3 unit to the terminal oxygen takes place via **TS29−30**; the intrinsic barrier amounts to 124 kJ mol^{-1}, which is 7 kJ mol^{-1} above the entrance channel and thus not accessible under thermal conditions. Furthermore, the intrinsic barrier for the subsequent proton transfer via **TS30−31** is ∼20 kJ mol^{-1} higher compared to the corresponding barrier of the $[VPO_4]^{\bullet+}/C_3H_8$ system. Next to the kinetic barrier, also the formation of the reaction products $[V_2O_4H_2]^{\bullet+}$(**32**)$/C_3H_6$ is more energy demanding compared to $[VPO_4H_2]^{\bullet+}$(**28**)$/C_3H_6$ resulting in an endothermicity of 4 kJ mol^{-1} for the ODH reaction. This holds also true as well for the competing hydride abstraction yielding neutral $V_2O_4H^{\bullet}$ and $[i\text{-}C_3H_7]^+$; this reaction path is endothermic by 50 kJ mol^{-1} and not accessible under thermal conditions.

With respect to the selectivity of the initial C−H bond activation step, we calculated the analogous reaction pathway for the $[VPO_4]^{\bullet+}/C_3H_8$ couple, in which the initial C−H bond scission takes place at a primary C−H bond (Figure 6).

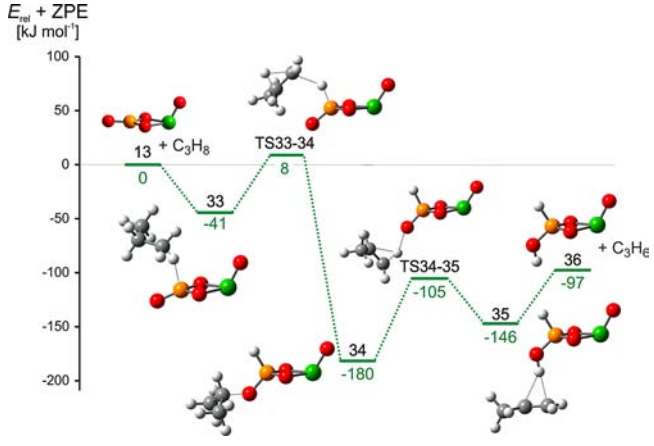

Figure 6. Simplified, electronic ground-state PES for the reaction of $[VPO_4]^{\bullet+}$ with C_3H_8 in which initial hydride transfer occurs from the primary position, calculated at the B3LYP/def2-TZVP level of theory (green, V; yellow, P; red, O; gray, C; white, H). The relative energies are given in kJ mol^{-1} and corrected for unscaled ZPE contributions.

However, the lowest transition structure for the C−H bond scission differs from the analogous **TS25−26** structure. After coordination of the hydrocarbon via the primary C−H bond (**33**, −41 kJ mol^{-1}), the transition structure **TS33−34** involves not only the hydride transfer to the phosphorus atom but also a [1,2]-hydrogen migration from the secondary to the primary position in the propane fragment, thus reflecting the intrinsic instability of a primary carbocation. As in intermediate **26**, the C3 unit is bound via a secondary carbon atom to the cluster, i.e., intermediates **34** and **26** correspond to rotational isomers along the C−O bond. As expected, the subsequent process **34** → **TS34−35** → **35** → **36** is almost identical to the

dx.doi.org/10.1021/ja400198y | J. Am. Chem. Soc. 2013, 135, 3711−3721

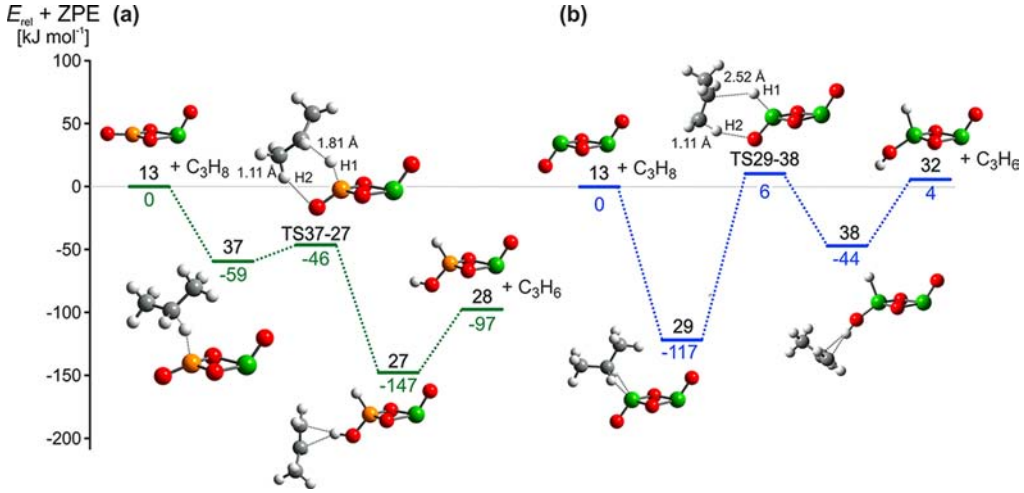

Figure 7. Alternative, "one-step" PESs for the reactions of (a) $[VPO_4]^{\bullet+}$ and (b) $[V_2O_4]^{\bullet+}$ with C_3H_8. All structures are calculated at the B3LYP/def2-TZVP level of theory (green, V; yellow, P; red, O; gray, C; white, H), and the relative energies are given in kJ mol^{-1} and corrected for unscaled ZPE contributions; the relevant C−H bond lengths are given in Å.

analogous reaction described above (Figure 5a), and the overall exothermicities forming the two products **28** and **36** are the same. However, the activation of a primary C−H bond in the first step is endothermic by 8 kJ mol^{-1} and accordingly not accessible under thermal conditions. This result apparently contradicts the reactivity with C_2H_6 in which the activation of primary C−H bonds is observed. However, the $[VPO_4]^{\bullet+}$/C_2H_6 couple gives rise to dehydrogenation, i.e., loss of neutral H_2, rather than oxidative dehydrogenation, i.e., the uptake of two hydrogen atoms, and another mechanistic scenario may account for this reactivity in which the formation of a hydride/hydroxyl species **36** is circumvented. Moreover, the branching ratio of 3% is very low, and this reactivity might also be traced back to the small fraction of ions possessing kinetic energies at the higher limit (see also Experimental Details section).

In addition to the two-step mechanism presented in Figures 5 and 6, an alternative one-step reaction pathway has been located as well (Figure 7). For example, the simultaneous activation of two C−H bonds via a six-membered ring is feasible. This process can be considered as a combined hydride/proton transfer from the hydrocarbon to the cluster unit; the Mulliken charges at the transferred hydrogen atoms H1/H2 in the corresponding transition structures **TS37−27** and **TS29−38** amount to −0.57/+0.21 and −0.45/+0.25 for the mixed V/P system (Figure 7a) and the pure vanadium system (Figure 7b), respectively, and the spin density remains in both cases at the remote vanadium atom. Furthermore, the progress of the hydride transfer in **TS37−27** and **TS29−38** is much more pronounced compared to the proton migration, as indicated by the respective C−H bond lengths (Figure 7), and the hydride transfer takes place preferably from the secondary position of C_3H_8.[105] For $[VPO_4]^{\bullet+}$, the rate-determining step of the one-step process of Figure 7a is only 2 kJ mol^{-1} less energy demanding than the one shown in Figure 5a; thus, both mechanisms of ODH are likely to occur. In contrast, for the $[V_2O_4]^{\bullet+}/C_3H_8$ couple, both transition structures **TS29−38** and **TS29−30** of the one- and two-step mechanisms, Figures 7b and 5b, respectively, are higher in energy compared to the entrance channel, in line with the experimental results.

Summarizing the mechanisms of both reaction couples $[VPO_4]^{\bullet+}/C_3H_8$ and $[V_2O_4]^{\bullet+}/C_3H_8$, the presence of phosphorus in the heteronuclear cluster provides the intrinsic prerequisites to enable the C−H bond activation of small hydrocarbons. However, the mechanistic details of the C−H bond fission described here are different compared to the hydrogen-atom transfer observed, e.g., $[V_xP_{4-x}O_{10}]^{\bullet+}$ with small hydrocarbons.[45,48,51,52,54] For the latter process, a high spin density at the abstracting atom is required,[53,106] while in the reaction of $[VPO_4]^{\bullet+}$ and $[V_2O_4]^{\bullet+}$ with propane, no unpaired spin density is located at the reactive site, and hydride instead of hydrogen-atom abstraction takes place with $[VPO_4]^{\bullet+}$ being the stronger hydride abstractor compared to $[V_2O_4]^{\bullet+}$.

4. SUMMARY AND CONCLUSION

The present work provides a model system for a chemical understanding at a molecular level for hydrocarbon oxidation by VPO catalysts, comparing the previously reported $[V_2O_4]^{\bullet+}$ ion and the newly generated $[VPO_4]^{\bullet+}$ cluster, investigated both experimentally and computationally. The latter cluster ion is generated by means of ESI of a mixed solution containing the two precursor compounds $VOCl_3$ and $PO(OEt)_3$; CID studies explain the fragmentation pathway of the observed V/P precursor ion all the way down to $[VPO_4]^{\bullet+}$. State-of-the-art IR photodissociation spectroscopy reveals that the cluster exhibits a four-membered ring structure with a terminal oxygen atom at each of the vanadium and the phosphorus centers, respectively; the P═O moiety is in plane with the four-membered ring, thus corresponding to a classical PO_3 unit. While $[V_2O_4]^{\bullet+}$ was found to be rather unreactive toward saturated and unsaturated hydrocarbons at thermal conditions, the $[VPO_4]^{\bullet+}$ ion brings about efficient oxidative dehydrogenation and hydride abstraction from propane and *n*-butane as well as oxygen atom transfer to ethene. The reactive site of the $[VPO_4]^{\bullet+}$ cluster in the OAT reaction with ethene corresponds to the P−O and not to the V−O unit, i.e., the transfer of an oxygen atom from the former to C_2H_4 is preferred due to the electrochemically favored reduction process $P^{+V} \rightarrow P^{+III}$ which can also explain the higher OAT reactivity of $[VPO_4]^{\bullet+}$ versus $[V_2O_4]^{\bullet+}$ possessing only V−O units. The presence of phosphorus in $[VPO_4]^{\bullet+}$ is also crucial in the oxidative dehydrogenation and hydride abstraction from propane. Again, the phosphorus site of the cluster constitutes the reactive site in that the phosphorus atom is the better hydride acceptor compared to vanadium; this advantage is also of importance for the ODH reaction.

dx.doi.org/10.1021/ja400198y | *J. Am. Chem. Soc.* 2013, 135, 3711−3721

Accordingly, the intrinsic property of phosphorus favoring two-electron reduction causes a tremendous effect on the reactivity and thus should be considered in upcoming investigation on gas-phase, condensed-phase, and surface-mediated bond activation processes, in which VPO and related heteronuclear oxide systems are being employed.

■ ASSOCIATED CONTENT

Supporting Information

Complete ref 75; comparison of TOF mass spectra of helium-tagged $[VPO_4]^{\bullet+}$ ions recorded after irradiation by an IR laser pulse, either with the laser wavenumber tuned off resonance or on resonance; and Cartesian coordinates for all optimized structures. This material is available free of charge via the Internet at http://pubs.acs.org.

■ AUTHOR INFORMATION

Corresponding Author

Maria.Schlangen@mail.chem.tu-berlin.de; asmis@fhi-berlin.mpg.de; Helmut.Schwarz@mail.chem.tu-berlin.de

Notes

The authors declare no competing financial interest.

■ ACKNOWLEDGMENTS

This work is supported by the Fonds der Chemischen Industrie, the Deutsche Forschungsgemeinschaft (DFG), and in particular the Cluster of Excellence "Unifying Concepts in Catalysis" (coordinated by the Technische Universität Berlin and funded by the DFG) as well as the National Science Foundation of China (21232001). Computational resources were provided generously by the Institut für Mathematik at the Technische Universität Berlin. We thank Prof. Martin Kaupp and Dr. Burkhard Butschke for helpful suggestions and discussions. L.J. and X.Z. are grateful to the Alexander von Humboldt-Stiftung for postdoctoral fellowships.

■ REFERENCES

(1) Limberg, C. *Angew. Chem., Int. Ed.* **2003**, *42*, 5932.
(2) Sauer, J. In *Computational Modeling for Homogeneous and Enzymatic Catalysis*; Morokuma, K., Musaev, J., Ed.; Wiley-VCH Verlag GmbH & Co. KGaA: Weinheim/New York, 2008, p 231.
(3) Gunay, A.; Theopold, K. H. *Chem. Rev.* **2010**, *110*, 1060.
(4) Bond, G. C.; Keane, M. A.; Kral, H.; Lercher, J. A. *Catal. Rev. Sci. Eng.* **2000**, *42*, 323.
(5) Zaera, F. *Top. Catal.* **2005**, *34*, 129.
(6) Ertl, G. *Angew. Chem., Int. Ed.* **2008**, *47*, 3524.
(7) Wachs, I. E. *Catal. Today* **2005**, *100*, 79.
(8) Ganduglia-Pirovano, M. V.; Popa, C.; Sauer, J.; Abbott, H.; Uhl, A.; Baron, M.; Stacchiola, D.; Bondarchuk, O.; Shaikhutdinov, S.; Freund, H.-J. *J. Am. Chem. Soc.* **2010**, *132*, 2345.
(9) Nilius, N.; Risse, T.; Schauermann, S.; Shaikhutdinov, S.; Sterrer, M.; Freund, H. J. *Top. Catal.* **2011**, *54*, 4.
(10) *Appl. Catal., A* **1997**, *157*, 1−425.
(11) Hutchings, G. J. *J. Mater. Chem.* **2004**, *14*, 3385.
(12) Millet, J.-M. *Top. Catal.* **2006**, *38*, 83.
(13) Taufiq-Yap, Y.; Goh, C.; Hutchings, G.; Dummer, N.; Bartley, J. *Catal. Lett.* **2009**, *130*, 327.
(14) Kourtakis, K.; Wang, L.; Thompson, E.; Gai, P. L. *Appl. Catal., A* **2010**, *376*, 40.
(15) Centi, G.; Trifiro, F.; Ebner, J. R.; Franchetti, V. M. *Chem. Rev.* **1988**, *88*, 55.
(16) Zhanglin, Y.; Forissier, M.; Sneeden, R. P.; Vedrine, J. C.; Volta, J. C. *J. Catal.* **1994**, *145*, 256.
(17) Cavani, F.; Trifiro, F. In *Catalysis*; Spivey, J. J., Agarwal, S. K., Eds.; The Royal Society of Chemistry: London, 1994; Vol. *11*, p 246.
(18) Chen, B.; Munson, E. J. *J. Am. Chem. Soc.* **1999**, *121*, 11024.
(19) Chen, B.; Munson, E. J. *J. Am. Chem. Soc.* **2002**, *124*, 1638.
(20) Kaczorowska, M.; Schwarz, H.; Schröder, D. *Eur. J. Inorg. Chem.* **2007**, *2007*, 3335.
(21) Cavani, F.; De Santi, D.; Luciani, S.; Löfberg, A.; Bordes-Richard, E.; Cortelli, C.; Leanza, R. *Appl. Catal., A* **2010**, *376*, 66.
(22) Böhme, D. K.; Schwarz, H. *Angew. Chem., Int. Ed.* **2005**, *44*, 2336.
(23) Lang, S. M.; Popolan, D. M.; Bernhardt, T. M. In *The Chemical Physics of Solid Surfaces*; Woodruff, D. P., Ed.; Elsevier: Amsterdam, 2007; Vol. *12*, p 53.
(24) Schröder, D.; Schwarz, H. *Proc. Natl. Acad. Sci.U.S.A.* **2008**, *105*, 18114.
(25) Johnson, G. E.; Tyo, E. C.; Castleman, A. W. *Proc. Natl. Acad. Sci.U.S.A.* **2008**, *105*, 18108.
(26) Schlangen, M.; Schwarz, H. *J. Chem. Soc., Dalton Trans.* **2009**, 10155.
(27) Roithová, J.; Schröder, D. *Chem. Rev.* **2010**, *110*, 1170.
(28) Schwarz, H. *Angew. Chem., Int. Ed.* **2011**, *50*, 10096.
(29) Zhao, Y. X.; Wu, X. N.; Ma, J. B.; He, S. G.; Ding, X. L. *Phys. Chem. Chem. Phys.* **2011**, *13*, 1925.
(30) Castleman, A. W. *Catal. Lett.* **2011**, *141*, 1243.
(31) Lang, S. M.; Bernhardt, T. M. *Phys. Chem. Chem. Phys.* **2012**, *14*, 9255.
(32) Schwarz, H.; Schlangen, M. *Catal. Lett.* **2012**, *142*, 1265.
(33) von Helden, G.; Kirilyuk, A.; van Heijnsbergen, D.; Sartakov, B.; Duncan, M. A.; Meijer, G. *Chem. Phys.* **2000**, *262*, 31.
(34) Asmis, K. R.; Brummer, M.; Kaposta, C.; Santambrogio, G.; von Helden, G.; Meijer, G.; Rademann, K.; Woste, L. *Phys. Chem. Chem. Phys.* **2002**, *4*, 1101.
(35) Oomens, J.; Sartakov, B. G.; Meijer, G.; von Helden, G. *Int. J. Mass Spectrom.* **2006**, *254*, 1.
(36) Asmis, K. R.; Fielicke, A.; von Helden, G.; Meijer, G. In *The Chemical Physics of Solid Surfaces*; Woodruff, D. P., Ed.; Elsevier: Amsterdam, 2007; Vol. *12*, p 327.
(37) Asmis, K. R.; Sauer, J. *Mass Spectrom. Rev.* **2007**, *26*, 542.
(38) Gruene, P.; Lyon, J. T.; Fielicke, A. In *Handbook of Nanophysics*; Sattler, K., Ed.; Taylor & Francis: 2010; Vol. *2*, p 9.
(39) Asmis, K. R. *Phys. Chem. Chem. Phys.* **2012**, *14*, 9270.
(40) Bell, R. C.; Zemski, K. A.; Kerns, K. P.; Deng, H. T.; Castleman, A. W. *J. Phys. Chem. A* **1998**, *102*, 1733.
(41) Zemski, K. A.; Justes, D. R.; Castleman, A. W. *J. Phys. Chem. A* **2001**, *105*, 10237.
(42) Engeser, M.; Schlangen, M.; Schröder, D.; Schwarz, H.; Yumura, T.; Yoshizawa, K. *Organometallics* **2003**, *22*, 3933.
(43) Justes, D. R.; Mitric, R.; Moore, N. A.; Bonačic-Koutecký, V.; Castleman, A. W. *J. Am. Chem. Soc.* **2003**, *125*, 6289.
(44) Moore, N. A.; Mitrić, R.; Justes, D. R.; Bonačić-Koutecký, V.; Castleman, A. W. *J. Phys. Chem. B* **2006**, *110*, 3015.
(45) Feyel, S.; Döbler, J.; Schröder, D.; Sauer, J.; Schwarz, H. *Angew. Chem., Int. Ed.* **2006**, *45*, 4681.
(46) Feyel, S.; Schröder, D.; Rozanska, X.; Sauer, J.; Schwarz, H. *Angew. Chem., Int. Ed.* **2006**, *45*, 4677.
(47) Wende, T.; Döbler, J.; Jiang, L.; Claes, P.; Janssens, E.; Lievens, P.; Meijer, G.; Asmis, K. R.; Sauer, J. *Int. J. Mass Spectrom.* **2010**, *297*, 102.
(48) Dietl, N.; Engeser, M.; Schwarz, H. *Angew. Chem., Int. Ed.* **2009**, *48*, 4861.
(49) Dietl, N.; Engeser, M.; Schwarz, H. *Chem.—Eur. J.* **2009**, *15*, 11100.
(50) Dietl, N.; Engeser, M.; Schwarz, H. *Chem.—Eur. J.* **2010**, *16*, 4452.
(51) Dietl, N.; Höckendorf, R. F.; Schlangen, M.; Lerch, M.; Beyer, M. K.; Schwarz, H. *Angew. Chem., Int. Ed.* **2011**, *50*, 1430.
(52) Ma, J. B.; Wu, X. N.; Zhao, X. X.; Ding, X. L.; He, S. G. *Phys. Chem. Chem. Phys.* **2010**, *12*, 12223.
(53) Dietl, N.; Schlangen, M.; Schwarz, H. *Angew. Chem., Int. Ed.* **2012**, *51*, 5544.

(54) Dietl, N.; Zhang, X.; van der Linde, C.; Schlangen, M.; Beyer, M. K.; Schwarz, H. *Chem. Eur. J.* **2013**, *19*, 3017.
(55) Wang, Z. C.; Wu, X. N.; Zhao, Y. X.; Ma, J. B.; Ding, X. L.; He, S. G. *Chem. Phys. Lett.* **2010**, *489*, 25.
(56) Nößler, M.; Mitrić, R.; Bonačić-Koutecký, V.; Johnson, G. E.; Tyo, E. C.; Castleman, A. W. *Angew. Chem., Int. Ed.* **2010**, *49*, 407.
(57) Wang, Z.-C.; Dietl, N.; Kretschmer, R.; Weiske, T.; Schlangen, M.; Schwarz, H. *Angew. Chem., Int. Ed.* **2011**, *50*, 12351.
(58) Ma, J.-B.; Wang, Z.-C.; Schlangen, M.; He, S.-G.; Schwarz, H. *Angew. Chem., Int. Ed.* **2012**, *51*, 5991.
(59) Ma, J.-B.; Wang, Z.-C.; Schlangen, M.; He, S.-G.; Schwarz, H. *Angew. Chem., Int. Ed.* **2013**, *52*, 1226.
(60) Schröder, D.; Weiske, T.; Schwarz, H. *Int. J. Mass Spectrom.* **2002**, *219*, 729.
(61) Cech, N. B.; Enke, C. G. *Mass Spectrom. Rev.* **2001**, *20*, 362.
(62) Zhang, X.; Schwarz, H. *Chem.—Eur. J.* **2010**, *16*, 1163.
(63) Due to the rather similar ion generation, both $[VPO_4]^{\bullet+}$ and $[V_2O_4]^{\bullet+}$ ions should undergo a comparable amount of collisions prior to entering the mass analyzer; thus the internal energy of both systems can be expected to be similar.
(64) Relative rate constants were obtained from experiments using 5 up to 10 different pressures in the range of 2×10^{-4} to 1×10^{-3} mbar. The slight increase of adduct formation with increasing pressure suggests that most likely multiple collisions account for their formation; this observation is in agreement with the identically observed adduct formation in the $[V_2O_4]^{\bullet+}/n\text{-}C_4H_{10}$ couple. It was also shown that for very reactive systems, efficient secondary reaction may take place: (a) Dietl, N.; Schlangen, M.; Schwarz, H. *Chem.—Eur. J.* **2011**, *17*, 1783. (b) Kretschmer, R.; Schlangen, M.; Schwarz, H. *Angew. Chem., Int. Ed.* **2012**, *51*, 3483 However, as shown by the kinetic analysis, single collsions prevail for the product formation in the reactions presented in this work.
(65) Schröder, D.; Schwarz, H.; Schenk, S.; Anders, E. *Angew. Chem., Int. Ed.* **2003**, *42*, 5087.
(66) Schröder, D.; Engeser, M.; Schwarz, H.; Rosenthal, E. C. E.; Döbler, J.; Sauer, J. *Inorg. Chem.* **2006**, *45*, 6235.
(67) Gruene, P.; Trage, C.; Schröder, D.; Schwarz, H. *Eur. J. Inorg. Chem.* **2006**, 4546.
(68) Zhang, X.; Schwarz, H. *ChemCatChem* **2010**, *2*, 1391.
(69) Chen, K.; Wang, Z.-C.; Schlangen, M.; Wu, Y.-D.; Zhang, X.; Schwarz, H. *Chem.—Eur. J.* **2011**, *17*, 9619.
(70) Kretschmer, R.; Schlangen, M.; Schwarz, H. *Angew. Chem., Int. Ed.* **2012**, *51*, 3483.
(71) Kretschmer, R.; Schlangen, M.; Kaupp, M.; Schwarz, H. *Organometallics* **2012**, *31*, 3816.
(72) Goebbert, D. J.; Meijer, G.; Asmis, K. R. *AIP Conf. Proc.* **2009**, *1104*, 22.
(73) Goebbert, D. J.; Wende, T.; Bergmann, R.; Meijer, G.; Asmis, K. R. *J. Phys. Chem. A* **2009**, *113*, 5874.
(74) Bosenberg, W. R.; Guyer, D. R. *J. Opt. Soc. Am. B* **1993**, *10*, 1716.
(75) Frisch, M. J. et al. *Gaussian 09*, revision A.1; Gaussian, Inc.: Wallingford, CT, 2009.
(76) Lee, C.; Yang, W.; Parr, R. G. *Phys. Rev. B* **1988**, *37*, 785.
(77) Becke, A. D. *J. Chem. Phys.* **1993**, *98*, 5648.
(78) Schäfer, A.; Huber, C.; Ahlrichs, R. *J. Chem. Phys.* **1994**, *100*, 5829.
(79) Fukui, K. *Acc. Chem. Res.* **1981**, *14*, 363.
(80) Gonzalez, C.; Schlegel, H. B. *J. Phys. Chem.* **1990**, *94*, 5523.
(81) Truhlar, D. G.; Gordon, M. S. *Science* **1990**, *249*, 491.
(82) *TURBOMOLE*, V6.2; University of Karlsruhe and Forschungszentrum Karlsruhe GmbH, 1989–2007, TURBOMOLE GmbH: Karlsruhe, Germany, 2010; http://www.turbomole.com.
(83) Grimme, S. *J. Comput. Chem.* **2006**, *27*, 1787.
(84) Weigend, F.; Ahlrichs, R. *Phys. Chem. Chem. Phys.* **2005**, *7*, 3297.
(85) Deglmann, P.; Furche, F.; Ahlrichs, R. *Chem. Phys. Lett.* **2002**, *362*, 511.
(86) Scott, A. P.; Radom, L. *J. Phys. Chem.* **1996**, *100*, 16502.
(87) Halls, M. D.; Velkovski, J.; Schlegel, H. B. *Theor. Chem. Acc.* **2001**, *105*, 413.
(88) Asmis, K. R.; Meijer, G.; Brummer, M.; Kaposta, C.; Santambrogio, G.; Woste, L.; Sauer, J. *J. Chem. Phys.* **2004**, *120*, 6461.
(89) Schröder, D.; Engeser, M.; Brönstrup, M.; Daniel, C.; Spandl, J.; Hartl, H. *Int. J. Mass Spectrom.* **2003**, *228*, 743.
(90) Such hexa-coordinated structural motives are quite common for vanadium centers in the oxidation state +IV, e.g., in aqueous $[VO(OH_2)_5]^{2+}$ or $[VO(OH)(OH_2)_4]^{+}$. In general, five- and six-coordinated vanadium cores prevail as dominant species in organometallic complexes of V^{IV} and V^{V}. For more details of the chemistry and structural features of vanadium complexes, see: Vanadium Compounds: Chemistry, Biochemistry, and Therapeutic Applications. *ACS Symposium Series 711*; Tracey, A. S., Crans, D. C., Eds.; American Chemical Society, Washington, D.C., 1998.
(91) Jiang, L.; Wende, T.; Claes, P.; Bhattacharyya, S.; Sierka, M.; Meijer, G.; Lievens, P.; Sauer, J.; Asmis, K. R. *J. Phys. Chem. A* **2011**, *115*, 11187.
(92) Podstawka-Proniewicz, E.; Piergies, N.; Skołuba, D.; Kafarski, P.; Kim, Y.; Proniewicz, L. M. *J. Phys. Chem. A* **2011**, *115*, 11067.
(93) Boczula, D.; Cały, A.; Dobrzyńska, D.; Janczak, J.; Zoń, J. *J. Mol. Struct.* **2012**, *1007*, 220.
(94) Schröder, D.; Schwarz, H. *Angew. Chem., Int. Ed.* **1990**, *29*, 1431.
(95) Roithová, J.; Schröder, D. *J. Am. Chem. Soc.* **2007**, *129*, 15311.
(96) Johnson, G. E.; Mitric, R.; Tyo, E. C.; Bonacić-Koutecký, V.; Castleman, A. W. *J. Am. Chem. Soc.* **2008**, *130*, 13912.
(97) NIST Computational Chemistry Comparison and Benchmark Database, *NIST Standard Reference Database Number 101*, release 15b; Johnson, R. D., III, Ed.; NIST: Gaithersburg, MD, 2011; http://cccbdb.nist.gov/.
(98) *CRC Handbook of Chemistry and Physics*, 69th ed.; CRC Press Inc.: Boca Raton, FL, 1988.
(99) Holmes, J. L.; Aubry, C.; Mayer, P. M. *Assigning Structures to Ions in Mass Spectrometry*; CRC Press, Taylor & Francis Group: Boca Raton, London, NY, 2007.
(100) Koch, W.; Liu, B.; Schleyer, P. v. R. *J. Am. Chem. Soc.* **1989**, *111*, 3479.
(101) Koch, W.; Schleyer, P. V.; Buzek, P.; Liu, B. W. *Croat. Chem. Acta* **1992**, *65*, 655.
(102) Chiavarino, B.; Crestoni, M. E.; Fokin, A. A.; Fornarini, S. *Chem.—Eur. J.* **2001**, *7*, 2916.
(103) Chiavarino, B.; Crestoni, M. E.; Fornarini, S.; Lemaire, J.; Mac Aleese, L.; Maître, P. *ChemPhysChem* **2004**, *5*, 1679.
(104) Anslyn, E. V.; Dougherty, D. A. *Modern Physical Organic Chemistry*; University Science Books: Sausalito, CA, 2006, p 87.
(105) The barrier for the coupled hydride/proton transfer from a primary/secondary C–H bond is 50 kJ mol^{-1} higher in energy compared to **TS37–27**; thus, only the reaction path starting with the hydride transfer from a secondary position is considered.
(106) Lai, W.; Li, C.; Chen, H.; Shaik, S. *Angew. Chem., Int. Ed.* **2012**, *51*, 5556.